THE JOURNAL OF PHYSICAL CHEMISTRY B
A JOURNAL OF THE AMERICAN CHEMICAL SOCIETY

pubs.acs.org/JPCB

Article

Direct Correlation between Short-Range Vibrational Spectral Diffusion and Localized Ion-Cage Dynamics of Water-in-Salt Electrolytes

Aritri Biswas and Bhabani S. Mallik*

Cite This: *J. Phys. Chem. B* 2023, 127, 236−248

Read Online

ACCESS | Metrics & More | Article Recommendations | Supporting Information

ABSTRACT: The molecular dynamics simulations of a "water-in-salt" electrolyte, lithium bis(trifluoromethyl sulfonyl) imide ($LiNTf_2$), with a varying concentration range of 3 to 20 m were performed to establish a direct connection between a dynamic property like the ion-cage lifetime with the short-range vibrational stretching frequency shift of the used probe, HOD. The properties reported here are compared to that obtained from experiments performed at the same concentrations. The time-series wavelet transform was adopted as a preferable mathematical tool for calculating the instantaneous fluctuating frequencies of the probe O−D stretch mode and the concentration-dependent vibrational stretch spectral signature based on the variable functions associated with a particular chemical bond derived from classical molecular dynamics trajectories. The decay time constants of frequency fluctuations and the lifetime of the ion cage (τ_{IC}) were estimated as a function of salt concentration. Herein, we emphasize the correlation between the slowest time constant (τ_3) of the decay of O−D stretch frequency fluctuations and the timescales associated with the lifetime of ion cages (τ_{IC}). The results exhibit that the existing relationships were also concentration-dependent. Therefore, this study highlights the connection between the ionic motions that regulate the overall system dynamics with the short-range vibrational frequency shift of the used probe, which was used similar to experiments. It also provides an understanding of the interionic interactions and the dynamical and spectral properties of the electrolytic mixtures. We establish a direct correlation between short-range frequency profile and localized ion-cage lifetime, which can fill the gap of understanding between viscosity, vibrational frequency, and ion-cage dynamics of electrolytes.

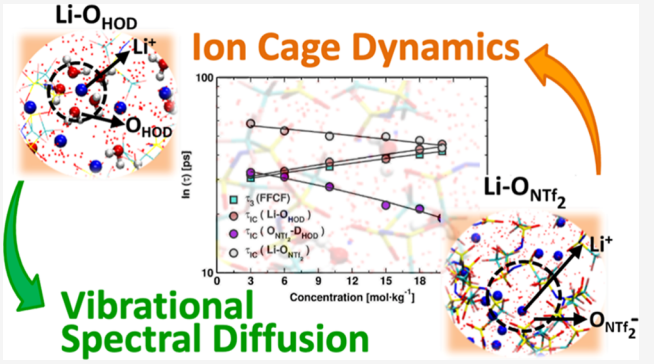

1. INTRODUCTION

Lithium-ion batteries (LIBs) are a significant source of electrochemical energy storage, powering our daily digital lives.[1,2] LIBs are extensively used in small electronic devices such as cell phones and computers because of their higher energy density, smaller size, and weight.[3−6] LIBs are growing in popularity for automotive applications to reduce greenhouse gas emissions and air pollution.[7] In between the electrodes, the principal component of LIBs is the electrolyte that helps conduct lithium ions.[2,8−10] The conventional electrolytic systems include organic carbonate solvents with high volatility and flammability, and the lithium-ion batteries based on these solvent electrolytes have safety issues.[11] However, the other most common electrolyte, $LiPF_6$, is thermally and electrochemically unstable. They tend to decompose at extremely high temperatures and absorb moisture, leading to HF formation that may corrode the battery constituents.[12,13]

Further, LIBs are far from their theoretical power density maximum; therefore, new developments are required to fill the scientific/technological gap.[14] Neglected areas in developing such storage devices are the choice of electrolytes that enhance the conduction ability of lithium ions and the modification of electrolytic composition to increase the efficiency, durability, and safety of an LIB. To address a few shortcomings in battery technology concerning high energy density, wide operating voltage windows, and safety issues,[15] aqueous electrolytes were introduced to solve the problems of electrochemical energy storage and conversion.[6,16,17] A slight variation in the composition of these aqueous electrolytes was expected to significantly alter the physicochemical properties and performance of these batteries. Moreover, the "water-in-salt" electrolytes within aqueous batteries[18,19] have recently attracted attention owing to their diversified use.[20,21] The water environment in aqueous electrolytes primarily impacts the properties to be tuned for applications and affects the

Received: June 24, 2022
Revised: December 14, 2022
Published: December 28, 2022

https://doi.org/10.1021/acs.jpcb.2c04391
J. Phys. Chem. B 2023, 127, 236−248

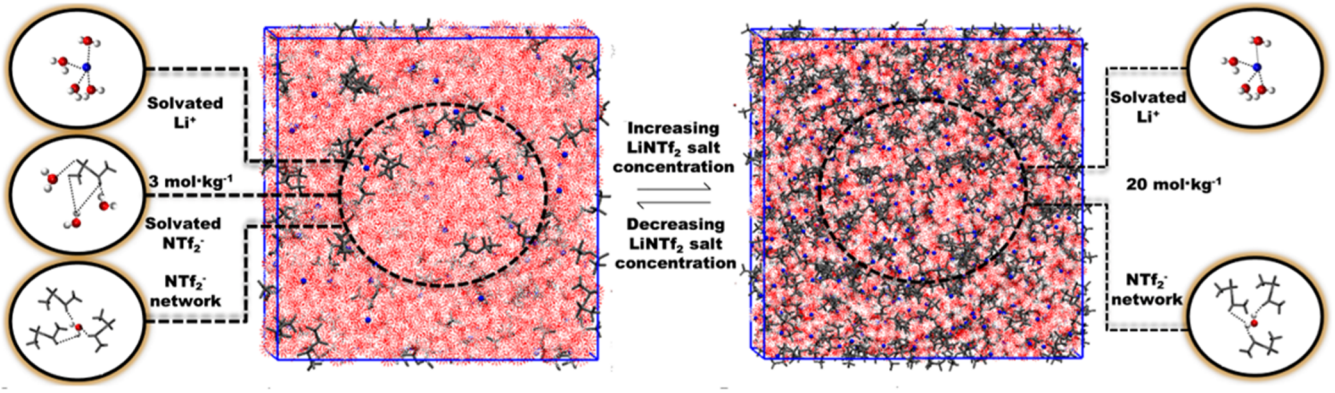

Figure 1. Snapshots of the cubic simulation box at a lower salt concentration, 3 mol kg^{-1}, and a higher concentration, 20 mol kg^{-1}.

reactivity. In the past, numerous experimental and theoretical investigations were reported using superconcentrated salts in aqueous solutions,[22] known as the "water-in-salt" electrolytes (WiSEs).[20,23] The reason behind the study of these electrolytic salt solutions is the ability of such superconcentrated electrolytes to enhance the window of electrochemical stability well beyond the thermodynamic limit of water, 1.23 V.[16] The difference in water speciation dictates reactivity and interfacial properties and expands the voltage window of aqueous electrolytic solutions.

Molecular dynamics (MD) simulations provide a fundamental understanding based on the molecular-level interpretation of the electrolytic properties in battery research.[24,25] Past studies reported several works on aqueous $LiNTf_2$ solutions focusing on transport property calculations,[6,26] exploring the heterogeneity in ionic liquid microstructures,[27,28] and studies relating to aqueous solution dynamics in highly concentrated electrolytic mixtures at varying salt concentrations.[29] With the combined efforts of infrared (IR) spectroscopic techniques and molecular dynamics (MD) simulations, it was observed that water molecules still seem to exhibit bulk-like behavior at ultrahigh concentrations of WiSEs, serving as a medium for ionic transport.[28] Herein, it was proposed that the solvated Li^+ moves through nanometric water channels, providing a mechanism of ion conduction in LIBs.[30] The other study employed small-angle neutron scattering (SANS) spectroscopy and molecular simulations to systematically study the structural variations within the ionic framework and the solvation and transport properties.[27] This work reported disruption of the cationic solvation structures, resulting in microstructural heterogeneity in conjunction with forming $Li(H_2O)_4^+$ that leads to faster transport of Li^+ due to higher transference numbers. However, several spectroscopic studies[31,32] demonstrated the local ordering and orientations of molecular structure and the dynamical properties in concentrated $LiNTf_2$–H_2O mixtures.[33,34] Still, this study might be helpful as it provides additional details that serve as the key to the structural understanding and dynamic exchanging of the ionic solvation behavior within aqueous $LiNTf_2$ solutions at various concentration regimes.

Moreover, conductivity is a critical property that depends on viscosity which can often limit the usefulness of these electrolytes and should be optimized for enhanced dynamics. Numerous studies to date focused on the influence of viscosity in the structural design and the reorganization dynamics of ILs.[35−38] Viscosity correlates well to the breakup of local ion cages that often lead to structural randomization of the coordinated environment.[37] Previous proceedings further suggested the connection between the experimentally measured longer picosecond timescale of IL reorganization with the calculated time constant of the dynamics of ion cages.[35,37−40] It was found that the longer timescale of spectral diffusion is in the same range as the relaxation timescale associated with the breaking and reformation of the ionic complexes that activate translational diffusion and determines viscosity. Therefore, one can understand the molecular origin of viscosity for extensive applications of these fluids as electrolytes. However, the correlation of ion-cage dynamics with other experimentally observed properties, like spectral profile, is not well established. It was proposed that the vibrational frequency shifts of the probe could be a better measure of ion pairing.[37] However, the direct one-to-one correlation has not been well presented in earlier studies. In the current study, we investigate the structural arrangement and molecular picture of the ionic solvation shells of "water-in-salt" electrolytic mixtures and aqueous $LiNTf_2$ solutions at six varying salt concentrations and the connection between dynamics and vibrational frequency. We focus on the dynamics of the lithium salt solutions by calculating the time-dependent frequency–frequency correlation functions (FFCFs) and ion-cage dynamics for a series of electrolyte compositions. We have reported the correlations between the changing composition and the changes in the timescales observed in the FFCFs, and the lifetime of ion cages. Both the frequency profile and ion-cage lifetime vary with electrolyte composition. Moreover, we establish a correlation between these two properties by employing MD simulations.

2. COMPUTATIONAL METHODS

We explore the dynamical response of the probe OD modes of HOD molecules in the solvated electrolyte system, similar to samples in ultrafast vibrational spectroscopy. The isotopically diluted deuterated hydroxyl (O–D) stretch modes serve as the sensitive reporter of the ultrafast dynamical transformations within the $LiNTf_2$ salt solutions. We simulated seven systems, 4% HOD–H_2O mixture along with 3, 6, 10, 15, 18, and 20 mol kg^{-1} aqueous $LiNTf_2$ salt solutions, each consisting of 100 HOD probe molecules using the classical MD simulation method. The electrolytic salt solutions of 3 and 6 mol kg^{-1} fall within the relatively lower concentration regime, and molal solutions beyond 10 mol kg^{-1} represent higher salt concentrations. The simulation parameters of the Li^+ ions were derived from the work of Lee and Rasaiah.[41] The flexible force field model with harmonic descriptions was adapted for

https://doi.org/10.1021/acs.jpcb.2c04391
J. Phys. Chem. B 2023, 127, 236−248

Scheme 1. Flowchart Representing the Theoretical Method Employed to Determine the Time-dependent Instantaneous Vibrational Stretching Frequencies of the Probe, Applying the Wavelet Transform of Classical Trajectories (WTCT).[55,56,a]

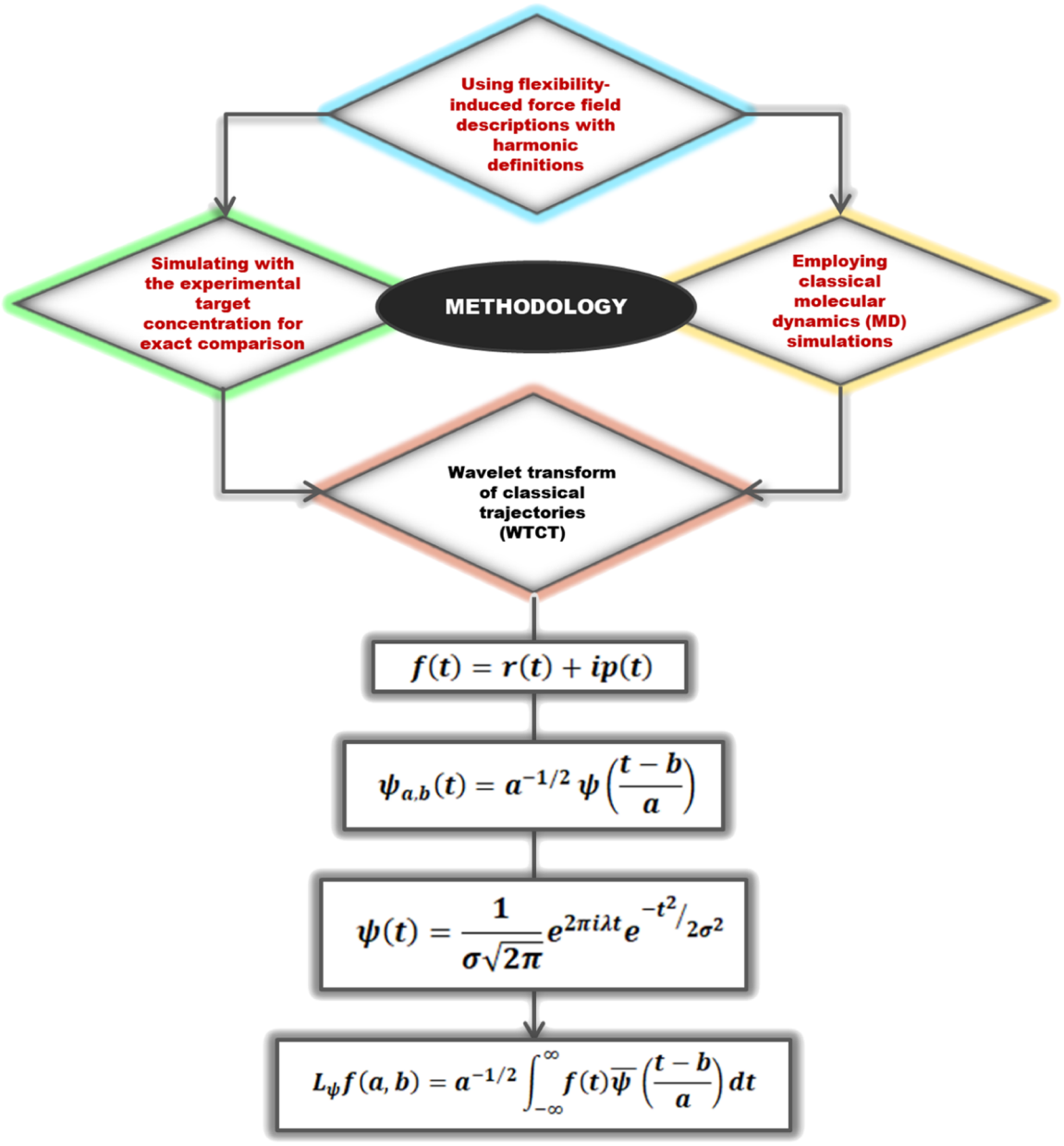

[a]In this scheme, a refers to the scale variable, b refers to the time variable, σ indicates the shape of the Gaussian time window, and λ denotes the center frequency.

the ionic liquid counteranion, NTf_2^- ion,[42] while the parameters of the simple point-charge water model (SPC-Fw)[43,44] were used for treating the probe and water molecules. Table S1 lists the non-bonded interaction parameters of HOD, water molecules, and ionic liquid $LiNTf_2$ contributing to the interatomic potential. We have presented the atomistic models of the packed contents at two different $LiNTf_2$ concentrations in Figure 1.

All molecular geometries were optimized using the Gaussian 09[45] software with the HF/6-31G (d) basis set. The random initial ionic structures were packed inside the cubic simulation box with the Packmol[46] software package. The energy of initial configurations was minimized with the steepest descent[47] integrator. The Particle Mesh Ewald (PME)[48−50] summation method with a cutoff value of 0.14 nm was employed to treat the long-range electrostatics and the van der Waals interactive forces. The equations of motion were integrated using the Verlet algorithm.[51] Further, two consecutive equilibration steps were carried out in an *NVT* ensemble, one at room temperature for 1 ns and the other at a higher temperature of 600 K for a total runtime of 2 ns. After the isothermal−isochoric (*NVT*) equilibration, the heated solution contents were brought back to room temperature in the *NVT* ensemble, following a stepwise procedure known as annealing. Next, the cooled constituents of the ionic mixtures were subjected to an isothermal−isobaric (*NPT*) simulation for 30 ns, subsequent *NVT* equilibration for a total duration of 50 ns, and further simulations in an NVE ensemble for 200 ns. The V-rescale[52] thermostat regulated the temperature of the solution contents during the *NPT* simulation, and the Parrinello−Rahman[53]

https://doi.org/10.1021/acs.jpcb.2c04391
J. Phys. Chem. B 2023, 127, 236−248

barostat maintained a constant pressure of 1 bar. During the simulation course, bonds containing hydrogen and deuterium atoms, except for the probe OD modes, were constrained with the LINCS algorithm.[54] The densities and box lengths calculated from the last 20 ns trajectory of the *NPT* simulation run are reported in Table S2. Finally, a production run was carried out for a total time of 1 ns. The final trajectories generated with a time step of 1 fs were utilized to calculate the instantaneous vibrational frequencies of the O−D stretch probe modes employing the wavelet method.[55,56] All MD simulations were performed with Gromacs version 5.1.2.[57−59] A flowchart representing the employed method is shown in Scheme 1.

The time-series wavelet transform (WT) is a preferable mathematical tool to calculate the fluctuating frequencies from variable functions associated with a particular chemical bond from the MD trajectories. Based on earlier reports, both the Laskar[60,61] approach and the Arevalo and Wiggins[56] method determine the instantaneous vibrational frequencies of the probe molecule in the complex molecular environment along the trajectory. The Laskar method divides the entire trajectory into several short time intervals. After that, the windowed Fourier transform generates the instantaneous vibrational frequencies in each short disjoint time interval. However, in the method of Arevalo and Wiggins, the time-dependent vibrational frequencies of the probe modes are calculated through the continuous WT of the trajectories. In all previous reports, the Arevalo and Wiggins[56] method has been used to calculate the time-dependent instantaneous fluctuating vibrational stretching frequencies and the normalized stretch frequency distribution.[62−67] The time-series WT is useful because the method automatically adjusts the time window size to the frequency of oscillations, providing better time localization and detailed spectral information than the Laskar method of the windowed Fourier transforms. In the wavelet method of Arevalo and Wiggins,[56] the Fourier transformation[68] of the time domain data generates the frequencies at each timestep.

The mathematical formulation of the wavelet theorem initiates the construction of a complex time-dependent function $f(t)$ consisting of the real and imaginary components, $r(t)$ and $ip(t)$, respectively

$$f(t) = r(t) + ip(t) \tag{1}$$

In the above expression, the real term $r(t)$ represents the instantaneous distance fluctuations along a specific bond vector and the imaginary constituent $ip(t)$ expresses the relevant relative momentum along the corresponding bond.

Next, in this method, the translations and dilations of the mother wavelet ψ are expressed in terms of two variables, the scale variable a, and the time variable b

$$\psi_{a,b}(t) = a^{-1/2}\psi\left(\frac{t-b}{a}\right)$$

2

To make the above equation useful, the a and b values of $\psi_{a,b}(t)$ were chosen such that ψ is real, $\psi_{a,b}(t)$ decays to 0 at $t \rightarrow \pm\infty$, and it satisfies the admissibility condition, $0 < c_\psi = 2\pi\int_{-\infty}^{+\infty}(|\hat{\psi}(\omega)|^2/|\omega|)d\omega < \infty$, wherein $\hat{\psi}$ represents the Fourier transform of ψ.

The WT of $f(t)$ determines the expansion coefficients in terms of a and b, according to the following equation provided $a > 0$, and b is real

$$L_\psi f(a, b) = a^{-1/2}\int_{-\infty}^{\infty} f(t)\overline{\psi}\left(\frac{t-b}{a}\right)dt \tag{3}$$

At each time interval $t = b$, the time−frequency representation of $f(t)$ stores local information in $L_\psi f(a,b)$. Hence, $L_\psi f(a,b)$ describes the frequency content in terms of variable parameters a and b. We perform our analysis using the Grossman−Morlet wavelet[69]

$$\psi(t) = \frac{1}{\sigma\sqrt{2\pi}}e^{2\pi i\lambda t}e^{-t^2/2\sigma^2} \tag{4}$$

In the above equation, the shape parameter σ^2 controlling the shape of the Gaussian time window and the center frequency λ could be readily varied. Mostly, the values of λ and σ considered were 1 and 2, respectively, and those values could be tuned to get a better resolution in the calculated frequencies.

In our calculations, we considered a periodic oscillatory function, $f(t) = e^{i2\pi\omega_0 t}$, and the WT of $f(t)$ employing eq 3 yields

$$\begin{aligned} L_\psi f(a, b) &= a^{-1/2}\int_{-\infty}^{\infty} e^{i2\pi\omega_0 t}\,\overline{\psi}\left(\frac{t-b}{a}\right)dt \\ &= a^{1/2}\int_{-\infty}^{\infty} e^{i2\pi\omega_0 as}\,e^{i2\pi\omega_0 b}\overline{\psi}(s)ds \\ &= a^{1/2}e^{i2\pi\omega_0 b}\overline{\psi}(\omega_0 a) \end{aligned}$$

wherein the modulus of WT $L_\psi f(a,b)$ is given by

$$|L_\psi f(a, b)| = \sqrt{a}\,\overline{\psi}(\omega_0 a) \tag{5}$$

In the above expression, $\overline{\psi}(\omega) = e^{-2\pi^2\sigma^2(\omega-\lambda)^2}$ and $\overline{\psi}$ provides for localization in frequency with the global maximum lying at $a\omega_0 = (1/2)[\lambda + \sqrt{\lambda^2 + (1/2\pi^2\sigma^2)}]$. Thus, the frequency variable defined with the Morlet−Grossman wavelet is as follows

$$\omega(t = b) = \frac{1}{2a}\left(\lambda + \sqrt{\lambda^2 + \frac{1}{2\pi^2\sigma^2}}\right) \tag{6}$$

Herein, we summarize the stepwise process of calculation of wavelet spectra. First, we compute the unit vector, that is, the intramolecular bond vector's distance and the corresponding bond's average distance. After that, we determine the time-varying distances of the probe and the corresponding distance fluctuations from the average value. Next, we determine the relative velocities and the projection of relative velocity along the specific bond. Henceforth, the relative velocities along the corresponding bond are multiplied by the reduced mass of the involved atoms to obtain the relevant momentum along the stretching mode. Subsequently, two scale values $\boldsymbol{a}1$ and $\boldsymbol{a}2$ that approximate the largest modulus of WT are estimated. Next, the moduli of the WT at scale value $\boldsymbol{a}$ and time value $\boldsymbol{b}$ are evaluated using Simpson's formula for numerical integration. After WT at each time window $\boldsymbol{t} = \boldsymbol{b}$, we get the instantaneous vibrational frequencies from the inverse of the scale factor $\boldsymbol{a}$. The scale value $\boldsymbol{a}$ governs the width of the time window. The small $\boldsymbol{a}$ value automatically narrows the time window at a high frequency and widens it at a lower frequency due to the large $\boldsymbol{a}$

https://doi.org/10.1021/acs.jpcb.2c04391
J. Phys. Chem. B 2023, 127, 236−248

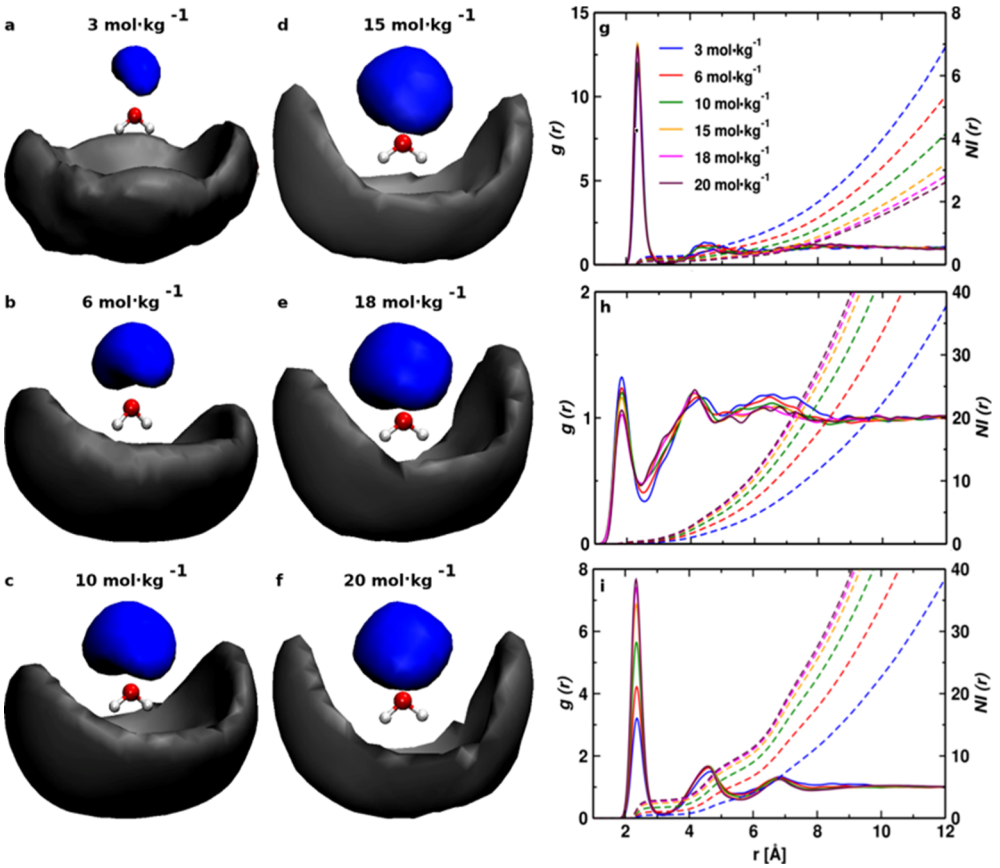

Figure 2. Computed SDFs (a–f) of the lithium cations (blue-colored isosurface, isovalue: 4.5) and NTf_2^- ions (black-colored isosurface, isovalue: 3.5) around the probe. The RDFs and NIs of (g) Li–O_{HOD}, (h) O_{NTf_2}–D_{HOD}, and (i) Li–O_{NTf_2} pairs at different $LiNTf_2$ salt concentrations.

value. Thus, WT runs repeatedly through the entire trajectory timeframe to calculate the vibrational stretching frequencies of the probe modes and determine the frequency distribution directly comparable to the experimental absorbance spectrum. Previously, the wavelet theorem had already been applied to determine the frequency distribution and examine the process of spectral diffusion in neat systems,[62,70] aqueous solvation shells,[64,71] solutions of neutral moieties,[63,72] and ionic liquid solutions.[67,73] We have presented a detailed discussion on the WTCT method employing classical MD simulations in our recent reports.[67,74−76]

3. RESULTS AND DISCUSSION

3.1. Structure of Aqueous Electrolytic Mixtures of Varying Compositions. ^{17}O nuclear magnetic resonance (NMR) spectroscopy study reported changes in the solvation shell of the lithium cation with a significant rise in the concentration of aqueous $LiNTf_2$ salt solutions.[20] Based on chemical shifts of the ^{17}O signal of water oxygen nuclei, the Li^+ ions were observed interacting with the lone pair on water oxygen. However, to understand the structure of the water-in-salt lithium-ion battery electrolytes, we calculated the spatial (SDFs) and radial (RDFs) distribution functions. We examine structural interactions within the ionic entities of the aqueous electrolytic solutions based on the corresponding SDFs and RDFs shown in Figure 2.

The atomic cloud density distribution in three-dimensional space was computed using the TRAVIS software package.[77] We examine the position of cations (represented by the blue-colored isosurface representation) and anions (represented by the black-colored isosurface representation) relative to the probe HOD molecule. Isosurface plots reveal the preferred cationic and anionic locations in 3D space; the oxygen atomic cloud interacts with the lithium cation, while the hydrogen and deuterium atoms are oriented toward the *bis*(trifluoromethylsulfonyl)imide anionic cloud. Herein, we examine that the gap between the blue isosurface lithium atom cloud and the oxygen of the probe decreases with an increase in the concentration of the $LiNTf_2$ salt solutions. However, the anionic density distribution is similar irrespective of the concentration rise of these aqueous electrolytic solutions. Thus, we infer enhanced ion-probe interactions within Li^+ and oxygen atomic cloud of the HOD probe molecule with an increase in salt concentration in these aqueous mixtures. Therefore, it might be crucial to inspect further the structural interactions from a cationic perspective based on the probe's dynamical and spectral response in different lithium salt solutions.

To further analyze the ionic structures, we analyze the Li–O_{HOD}, O_{NTf_2}–D_{HOD}, and Li–O_{NTf_2} RDFs and the corresponding number integrals (NIs) for characterizing the structural environment of the liquid salt around the vibrational reporters. For the cation-probe structural interactions between Li^+ and the oxygen atom of the probe HOD molecules, a significant difference lies at the well depth of the first RDF peak minimum and the peak maxima corresponding to the second solvation shell, hinting at long-range electrostatic correlations. The minimum depth between the first and second solvation shells suggests the strength of hydrogen-bonding structural inter-

https://doi.org/10.1021/acs.jpcb.2c04391
J. Phys. Chem. B 2023, 127, 236−248

actions. Therefore, the Li−O_{HOD} RDFs depict well-structured interactions with an increase in salt concentration. However, a slight variation in the peak heights and the well depth of the first minimum of the O_{NTf_2}−D_{HOD} RDFs is observed as a function of concentration. Our results indicate that the strength of anion−probe interactions is weaker in the superconcentrated solutions (~20 m) than in dilute ones. Besides, the interaction between lithium cation and the specific oxygen site of the NTf_2^- ion decreases with an increase in concentration owing to the increase in relative probabilities at the first peak minimum. The number integral values follow a specific trend; the predicted numbers decrease for the cation−probe interactions with increased $LiNTf_2$ salt concentrations. In contrast, the coordination numbers predicted for the site-specific anion−probe and cation−anion interactions are higher for the superconcentrated solutions.

Based on the above observations, we elucidate that lithium ion strongly interacts with the lone pair of electrons on the oxygen atom of the HOD probe molecule, complementing our SDF data. Based on well depth at the first minimum of the RDF plots, the cation−anion interactions within the aqueous ionic mixtures are more pronounced than the ion−probe interactions in previously reported solutions.[78−80] Moreover, past studies[20,81−83] revealed the lithium-ion solvation sheath structure—in the dilute regime, Li^+ coordinates with at least four solvent water molecules within the solvation shell, and the ion NTf_2^- remains hydrophobic.[81] However, as the weight or volume of salt outnumbers the solvent in WiSEs, water molecules tend to associate with Li^+ and form relatively long-lived $Li(H_2O)_n^+$ complexes owing to strong ion−water interactions.[20,82] However, we observe enhanced ion−water interactions relative to water−water associations in solution with an increase in salt concentration. Also, computer simulations further suggested a quasi-solvate ionic liquid structure composed of $Li(H_2O)_n^+$ weakly bound to the anionic counterpart at high salt concentrations.[83] Besides, force-field-based classical MD simulations portraying ion−water correlations throughout the concentration range depicted the formation of anionic nanodomains that weakened cation−anion correlations at higher salt molalities, leading to larger values of the Li-ion transport numbers well in agreement with our RDF data.[16,26] Previously, synchrotron X-ray spectroscopy (SAXS) was used to investigate the structural variation of the NTf_2^- ion over the whole concentration regime.[10] This study revealed different anionic solvation behaviors at low, medium, and high concentrations. At a relatively lower salt concentration (~1 m), NTf_2^- solvated structures exist owing to the solvation of the anionic species by bulk water molecules. However, the structural exchange as a function of concentration and temperature results in the coexistence of solvated NTf_2^- and network structures formed through hydrogen bond associations within the anion and interfacial water at a medium concentration range (~2−15 m). With a further increase in concentration beyond 15 m, the NTf_2^- solvated structures gradually disappear, and the anionic network structure comes into the picture at a higher concentration solution regime (~20 m).

3.2. Vibrational Stretch Spectral Signature and the Frequency Distribution. Figure 3 represents the normalized stretch frequency distribution of the OD bonds of the probe at different $LiNTf_2$ concentrations, applying the wavelet method.[55,56] The peak position of maximum intensity in the normalized O−D stretch frequency distribution of 4% HOD−H_2O solution represents a principal spectral peak centered at 2510 cm^{-1}. In contrast, the calculated O−D stretch signatures of 3, 6, and 10 mol kg^{-1} aqueous solutions depict a bimodal spectral line shape. The asymmetric line shape represents a peak for the O−D stretching vibrations around 2510 cm^{-1}, corresponding to water−water hydrogen bond associations like the bulk water. Gradually, a peak develops along the blue side of the spectrum centered at 2630 cm^{-1} with an increase in the $LiNTf_2$ concentration representing the anion-bound population of the deuterated hydroxyls. The blue shift also indicates weaker hydrogen-bonding associations in the lithium salt solution relative to bulk water. Thus, the peak due to the water−water hydrogen-bonding network completely disappears in the water-in-salt regime with an increase in concentration beyond 15 m. We also observe the frequency profile of the OD stretching vibrations to shift toward the blue side of the spectrum with an increase in the bulk $LiNTf_2$ concentrations. The blue shift in the spectral peak indicates that the water-associated deuteroxyl population hydrogen-bonded to the vicinal water molecules gets distorted with an increase in the concentration of the lithium salt solutions. It is also important to note that the ion-bound water population is weakly hydrogen-bonded compared to the water molecules hydrogen-bonded with the surrounding solvent water within the ionic framework. The calculated linewidth of the water-associated spectral peak is approximately 140 cm^{-1}, and the width of the spectral line shape of the anion-bound deuteroxyl population is about 60 cm^{-1}. For the aqueous mixtures, the peak positions of maximum intensity and the linewidth of the spectral peak in the computed frequency distribution correlate with the experimentally reported peak center frequency, ~2510 cm^{-1} (bandwidth 140 cm^{-1}) for the water-associated water population and ~2630 cm^{-1} (bandwidth 60 cm^{-1}) for the water molecules hydrogen-bonded to the NTf_2^- ions.[84] Our findings match well with the experiment.[28] Based on another report, increasing salt concentrations from 1 to 21 m, the intense peak at 2510 cm^{-1} representing HOD···OH_2 species in the FT IR absorption spectra fades. However, the peak at 2630 cm^{-1} assigned to HOD···NTf_2^- population gets intensified.[85,86] This study further emphasized that the spectral band at 2630 cm^{-1} is independent of the cationic influence but appears due to hydrogen bond associations between the D atom of the HOD probe molecule and the sulfonyl oxygen atoms, O−D···O═S, of NTf_2^- ion.

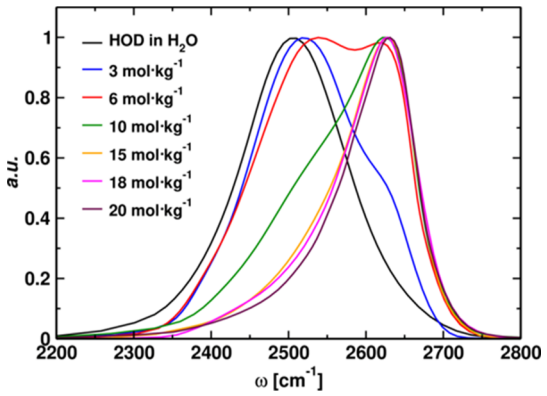

Figure 3. Normalized frequency distribution of the OD stretch probe modes in 4% HOD−H_2O mixture and aqueous electrolytic solutions at varied salt molalities.

https://doi.org/10.1021/acs.jpcb.2c04391
J. Phys. Chem. B 2023, 127, 236−248

3.3. Dynamics of Frequency−Time Correlation versus Ion-Cage Dynamics in the Aqueous Ionic Framework.

We calculated the frequency−frequency correlation function (FFCF) expressed as $C_\omega(t)$ that estimates the sub-picosecond dynamics of the associated system

$$C_\omega(t) = \frac{\langle \delta\omega(t)\delta\omega(0)\rangle}{\langle \delta\omega(0)^2\rangle} \tag{7}$$

In the above equation, $\boldsymbol{C_\omega(t)}$ refers to the decay of time−frequency representations, and $\boldsymbol{\delta\omega(t)}$ yields the instantaneous shift in frequency from the average value. The frequency of the vibrational chromophore is sensitive to its local environment. The probe modes oscillate at a particular intrinsic frequency at an initial instant. With time, differential site-specific interactions of the probe with the vicinal environment result in vibrational frequency changes, which causes vibrational spectral diffusion.[62,63,87−91] Further, infrared (IR) probes[37,92−98] interrogate spectral diffusion dynamics[74,91,99−104] based on their structural and dynamical response within the aqueous ionic framework. However, aqueous ionic dynamics within the liquid microenvironment are governed by ionic motions relating to the disruption and reformation of the hydrogen-bonded structural configurations. Experiments suggested the existence of neutral aggregates within the aqueous ionic mixtures.[105,106] The ions within the electrolytic solutions are held together by the electrostatic Coulombic forces. The concept of ion pairing (ions present in close vicinity) is highly ambiguous at extremely high ionic concentrations.[107−109] In such a scenario, the ion cage definition might be appropriate to understand ionic dynamics within the solvated environment.[6,38,40,110,111] The idea of ion-cage dynamics was conceptualized based on Luzar and Chandler's method[112−114] of determining hydrogen bond dynamics. Therefore, to calculate the continuous lifetimes of the hydrogen-bonded pairs, the population variable parameter $\boldsymbol{h(t)}$ is defined based on interactions within the ionic entities. Similarly, the ion-cage lifetime is computed by fitting the following time correlation function[38,40,108,109]

$$\boldsymbol{S_{IC}(t)} \approx \frac{\langle \boldsymbol{h(0)h(t)}\rangle}{\langle \boldsymbol{h}\rangle} \tag{8}$$

Herein $\boldsymbol{h(t)}$ is unity if the ionic groups are within a particular cutoff radius at a time $\boldsymbol{t}$ and 0 otherwise if the ion leaves the first solvation shell. This work unveils the relationship between the relaxation time constant of the long decay component of the time-dependent frequency fluctuations and the timescale associated with the breakup of local ion cages employing classical simulations. The frequency correlation function decay is further fitted with a triexponential fitting function shown below to yield the dynamical timescales associated with the fluctuating frequencies of the OD bonds in the water-in-salt mixtures listed in Table 1. The triexponential function best fits the calculated decay curves

$$\boldsymbol{X(t) = a_1 e^{-t/\tau_1} + a_2 e^{-t/\tau_2} + a_3 e^{-t/\tau_3}} \tag{9}$$

The spectral diffusion quantified by the decay of FFCFs shown in Figure 4 provides an insight into water dynamics associated with ultrafast molecular motions. Spectral dynamics in these aqueous ionic mixtures depict three timescales: a rapid initial fast decay timescale indicating the local structural fluctuations of the intact hydrogen-bonded configurations, followed by the intermediate decay time constant corresponding to more significant length-scale fluctuations about the hydrogen bond networks[115,116] and the slowest timescale representing the exchange of the hydrogen-bond partners accompanied by large angular jumps.[86,117] A past study[28] revealed the rotational relaxation time constants of the anisotropy IR pump−probe signals, wherein the faster time constant approximately varying within the range of 1 ps originating from the inertial rotational motion of the OD groups in the restricted ionic environment is observed to be independent of the $LiNTf_2$ concentration. However, the slowest timescale (∼17 ps) associated with the large amplitude rotational diffusion becomes further slower with increased concentration. Also, the longest decay time component of the anisotropy decay agrees with the slowest spectral diffusion relaxation timescale of the fluctuating OD stretch modes. Further, the time-dependent experimental nodal line slope (NLS) after being fitted with the biexponential function depicted two timescales, a faster component (1.1 ps) and a slower relaxation time constant (13.4 ps). Our calculated faster FFCF decay timescale is similar to the aqueous $LiNTf_2$ solutions. However, the intermediate and longer decay time constants gradually lengthen with an increase in concentration, indicating sluggish dynamics at higher salt molalities. Hence, the changes in local molecular structure induced by the modification of the hydrogen-bonding networks govern the overall dynamical transformations within the aqueous electrolytic framework.

To further obtain time-resolved information about the ionic solvation state and its dynamic correlations with the local environment, we determine the lifetime of ion cages in the

Table 1. Time Constants in Picoseconds Obtained by Fitting the Decay of the Frequency−Frequency Time Correlation Functions Are Listed Below

	frequency−frequency correlation function, $C_\omega(t)$					
concentration (mol kg^{-1})	τ_1	τ_2	τ_3	a_1	a_2	a_3
3	0.49	2.38	30.57	0.38	0.51	0.11
6	0.52	3.41	32.41	0.44	0.23	0.33
10	0.65	4.99	34.96	0.52	0.28	0.20
15	0.82	5.93	38.39	0.50	0.27	0.23
18	0.96	6.87	40.32	0.48	0.35	0.17
20	1.03	7.82	41.91	0.36	0.49	0.15

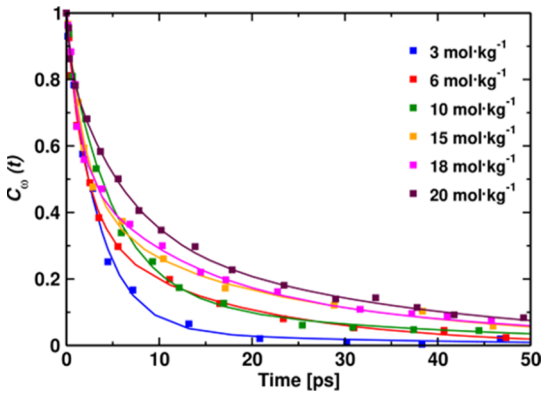

Figure 4. Time-dependent decay of frequency correlation at various $LiNTf_2$ salt concentrations. The raw data are shown with squares, while the solid lines depict triexponential fits to the calculated data sets.

https://doi.org/10.1021/acs.jpcb.2c04391
J. Phys. Chem. B 2023, 127, 236−248

super concentrated salt water electrolytic systems. The concerned times are obtained by fitting the corresponding autocorrelation function decay curves with the stretched exponential fitting function as follows

$$Y(t) = a_0 e^{(-t/\tau_{IC})^{\alpha}} \quad (10)$$

In the above expression, τ_{IC} represents the lifetime associated with the dynamics of the local ion cages. The formation of ion cages within the aqueous solutions depicts long-range structural ordering. At a relatively high $LiNTf_2$ salt concentration, the probe HOD molecules are expected to be intercalated within the Li^+ and NTf_2^- ionic aggregates. The time the ions stay in proximity within the cage describes the overall dynamics of the associated electrolytic solutions. The ion cages are defined based on the cutoff distance of the first RDF peak minimum of the corresponding pair of the central ion and the surrounding counterions.[40,118] Moreover, the microscopic system dynamics in the liquid phase are governed by the breaking and reformation of ion complexes. Therefore, we calculated the ion-cage correlation functions of Li−O of HOD, O of $[NTf_2]$−D of HOD, and Li−O of NTf_2^- ions to explore the probability of the corresponding ions staying within a certain cutoff distance from the reference ion. Herein, the continuous-time correlations of the ion-cage formation were determined and are shown in Figure 5 to explore the escape dynamics from the caged structure.[39,119]

We investigate the time the Li^+ and NTf_2^- ion stay in the vicinity of the probe molecules and the lifetime of the cation−anion correlations between the lithium cation and the oxygen site of the NTf_2^- ion. The radial distance cutoff for these calculations is taken from the pair correlation curves, $Li-O_{HOD}$ (3.25 Å), $O_{NTf_2}-D_{HOD}$ (2.75 Å), and $Li-O_{NTf_2}$ (3.30 Å) RDFs presented in the earlier part of the paper. The fitting parameters of the autocorrelation functions are listed in Table 2. For the Li^+-O_{HOD}, we observe an increase in ion-cage lifetime values when the concentration increases. Based on the RDF data, the computed results match well with our earlier observations wherein we examine enhanced structural interactions between the probe HOD and lithium cations within the electrolytic solutions at higher salt concentrations. An increased number of vicinal anions at higher salt molalities make it difficult for Li^+ to leave the ionic solvation and stay trapped inside the cage for an extended period. Besides, the increase in salt concentration slows down the motion of lithium ions, so they take more time to leave the ion cage. For the site-specific anion−probe ($O_{NTf_2}-D_{HOD}$) and the cation−anion ($Li-O_{NTf_2}$) caged complex, the time the ions remain trapped inside the ion cage before escaping out decreases with an increase of concentration. Thus, it takes lesser time for the NTf_2^- ions to hop out of the caged structure at higher salt concentrations. Our observations match the strength of the ion−probe and cation−anion structural interactions predicted by the spatial and radial distribution functions. SDF plots reveal the atomic cloud of the probe oxygen oriented toward Li^+, while the deuterium or hydrogen atoms of the HOD probe molecules are directed toward the anionic density distribution. Also, the strength of structural correlations between the probe HOD and lithium cations increases with an increase in concentration, and the pronounced interaction prevents the escape of the probe HOD molecules from the $Li-O_{HOD}$ caged complex. However, the anion−probe structured interactions

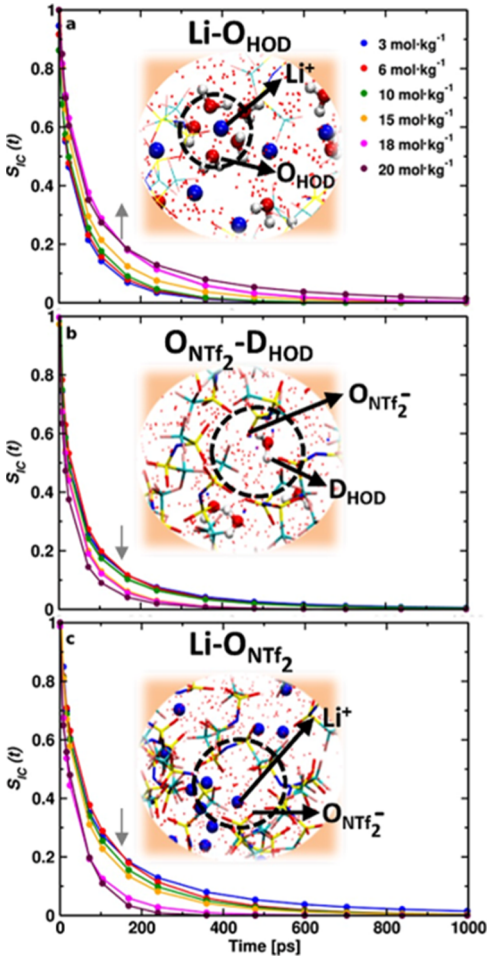

Figure 5. Time-dependent decays of the (a) $Li-O_{HOD}$, (b) $O_{NTf_2}-D_{HOD}$, and (c) $Li-O_{NTf_2}$ ion-cage correlation functions at varying salt concentrations. The dotted lines show the raw data, while the solid lines depict the fitted data, fit by a stretched exponential fitting function. The inset of each figure displays the structural snapshots from MD simulations depicting orientations of the HOD probe molecule relative to Li^+ and NTf_2^- ions and the conformation of Li^+ cations and NTf_2^- ions within the ion cage.

within the oxygen atom of NTf_2^- ions and the deuterium of probe ($O_{NTf_2}-D_{HOD}$) based upon the isosurface plots are almost similar irrespective of salt concentration, indicating faster movement of the anions than the cations from the ion-probe local ion cages. Moreover, the pair correlation curves of the anion−probe interactions suggest weaker interactive associations relative to the cation−probe structured interactions, in agreement with the ion-cage dynamical predictions.

4. CONCLUSIONS

An MD simulation study was carried out on $LiNTf_2-H_2O$ mixtures to examine the microstructural aspects and ultrafast dynamical changes within the lithium solvation structure due to the formation of two separate domains: the aqueous (water-associated water population) and anionic nanostructured (anion-associated water population) domains. $LiNTf_2$ was the chosen aqueous electrolytic system for this study due to its high water solubility and thermal and electrochemical stability at high molal (m) concentrations. Water-in-lithium salt is the chosen electrolyte in this study for battery applications. It is an

https://doi.org/10.1021/acs.jpcb.2c04391
J. Phys. Chem. B 2023, 127, 236−248

Table 2. Picosecond Time Constants of the Li−O_{HOD}, O_{NTf_2}−D_{HOD}, and Li−O_{NTf_2} Ion-Cage Autocorrelation Functions at Various $LiNTf_2$ Salt Concentrations and the Correlation Coefficients (χ^2) Are Listed Here

$S_{IC}(t)$	concentration (mol kg^{-1})	a_0	τ_{IC}	α	χ^2
Li−O_{HOD}	3	0.75	31.84	0.52	0.92
	6	0.68	33.02	0.67	0.94
	10	0.86	36.80	0.59	0.95
	15	0.54	38.39	0.63	0.92
	18	0.82	42.78	0.70	0.94
	20	0.78	45.41	0.55	0.94
O_{NTf2}−D_{HOD}	3	0.52	32.60	0.48	0.96
	6	0.68	30.98	0.57	0.95
	10	0.74	27.54	0.74	0.94
	15	0.86	22.17	0.66	0.97
	18	0.63	21.26	0.59	0.98
	20	0.73	19.06	0.62	0.96
Li−O_{NTf2}	3	0.61	58.06	0.58	0.95
	6	0.54	53.27	0.69	0.93
	10	0.78	50.02	0.50	0.96
	15	0.67	49.65	0.57	0.97
	18	0.82	47.47	0.71	0.92
	20	0.59	43.53	0.74	0.95

alternative to conventional organic electrolytes owing to its nonflammability and enhanced electrochemical stability window. The structural modification of the aqueous hydrogen-bonding environment within the Li^+ solvation sheath impacts the performance of WiSEs.[20] Also, water speciation due to the distinct arrangement and size of nanostructures in highly concentrated $LiNTf_2$-based water-in-salt systems drastically changes the physicochemical properties.

The OD stretch probe modes of the HOD molecule sensitively report associated system dynamics through hydrogen-bonding structural interactions with the vicinal ions in the aqueous $LiNTf_2$ solutions. This study provides a detailed description of the Li^+ solvation structure and solution dynamics. Water molecules tend to solvate the cationic species in dilute salt solutions, forming a sheath structure. At a lower salt concentration regime of 3 mol kg^{-1}, the Li^+ ions are bound to the solvent water molecules within the solvation sheath, and the NTf_2^- ions are weakly bound. Water molecules are free at a relatively lower concentration in the aqueous ionic mixtures. However, the scarcity of solvent water transforms the Li^+ solvation sheath structure with a further increase in salt concentration beyond a concentration range of 10 mol kg^{-1}. Herein, water molecules associate with the anionic constituent of the electrolytic solutions to form anion-bound water structures at higher salt concentrations above 10 mol kg^{-1}. Thus, the normalized distribution of the OD stretch probe modes in the $LiNTf_2$−water mixtures at higher salt molalities mainly exhibits effects due to interactions with the NTf_2^- ions. Based on the previous experimental studies[120,121] and MD simulation results,[67] it was observed that the anion-bound deuterated hydroxyls dominated the stretch spectral signature in the ionic systems more than the contribution from the cationic counterpart. A peak develops on the blue side of the stretch spectral signature of the bulk water molecules in the frequency distribution owing to the structured interactions of the anion-bounded OD pairs. In contrast, a change in the cationic constituent keeping the same anionic counterpart results in a shift of the spectral band toward a higher or lower wavenumber, depending on the type of IL constituting the cation. In this study, we take up different aqueous $LiNTf_2$ salt solutions at varied concentrations; as a result, we do not examine cation-dominated spectral changes based on the response of the local OD probe modes.

Also, we calculated the longest picosecond FFCF timescale (τ_3) and the lifetimes of the caged ionic complexes (τ_{IC}) at multiple salt concentrations. It is observed that the slowest timescale (τ_3) of frequency fluctuations indicates the escape dynamics of ions out of the caged complexes. The ion-cage structure and the escape dynamics after the breakup of the local ion cages are expected to play an essential role in determining the ionic transport properties relevant to battery functions. Ionic conductance and viscosity further regulate the extent of molecular motions in the liquid medium. The electrochemical performance[122,123] of the lithium electrolytic solution depends on ionic conductivity. Higher conductivity and lower viscosity facilitate faster ionic transport and enhance battery performance. The lifetime of the caged ionic complex also dictates ion transport in electrolytes. A longer lifetime of the ions within the cage results in slower escape events, leading to sluggish dynamics. The breakup of the caged complex influences the diffusivity of ions that determines transport within the electrolytic mixtures. All these properties of the battery electrolytes further govern ionic dynamics and largely affect the performance of LIBs. Several past studies proposed the computed lifetime of ion cages to be correlated to the slowest timescale of frequency fluctuation time correlation functions derived from ultrafast experiments.[39,40] This study determines the time-dependent dynamics of Li−O_{HOD}, O_{NTf_2}−D_{HOD}, and Li−O_{NTf_2} ion cages, the escape of counterions, HOD probe molecules, and the NTf_2-ions out of the solvation shell of the Li−O_{HOD}, O_{NTf_2}−D_{HOD}, and Li−O_{NTf_2} caged complexes. Herein, we draw attention to the existing correlation and the dynamical trends by computing these properties for the water-in-salt lithium *bis*(trifluoromethyl sulfonyl)imide solution as a function of salt concentration. We solely employed classical MD simulations for the first time to obtain the relationship between the longest time constant of the frequency−time correlation functions and the lifetime of ion-cage formation. The data sets are presented in Figure 6.

At lower salt concentration ranges of 3 and 6 mol kg^{-1}, the calculated slowest time constant obtained from the decay fit of the FFCF curve is approximately the same as the lifetime of Li−O_{HOD} and O_{NTf_2}−D_{HOD} ionic species. In comparison, the timescale of the Li−O_{NTf_2} cage is relatively longer when the concentration of the salt solution is 3 mol kg^{-1}. Moreover, it is observed that the longer time decay component of frequency fluctuations (τ_3) and the lifetime of the Li−O_{HOD} caged complex increase with an increase in the molal salt concentration. This observation hints at slower dynamics of the probe O−D modes with an increase in the lithium salt concentration. Further, the results imply that cation−probe interactions between Li^+ and the specific oxygen site of the probe HOD molecules within the ion cage directly modulate the time-dependent instantaneous fluctuating frequencies of the OD bonds. However, for the anion−probe (O_{NTf_2}−D_{HOD}) and cation−anion (Li−O_{NTf_2}) correlations, the time taken to restructure the ion complexes decreases with an increase in $LiNTf_2$ concentration. Thus, the breakup of the local ion cages

https://doi.org/10.1021/acs.jpcb.2c04391
J. Phys. Chem. B 2023, 127, 236−248

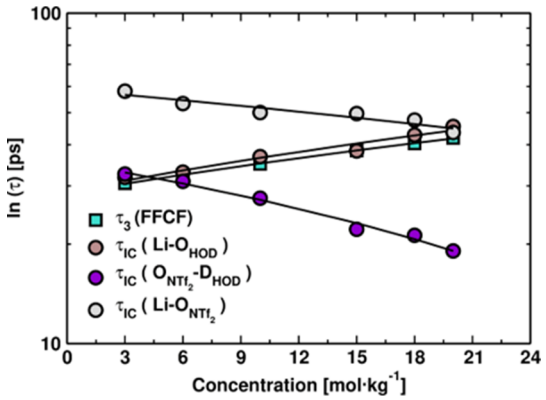

Figure 6. Relation between the calculated slowest timescale of the decay of instantaneous frequency fluctuations of the OD bond (τ_3) and the picosecond relaxation time constant (τ_{IC}) associated with the formation of ion cages versus concentration (mol kg^{-1}). The straight line depicts a linear fit to the computed data sets.

governs molecular diffusion and determines viscosity trends. A linear relationship was found between the calculated quantities, τ_3, of FFCFs and lifetime of ion cages, τ_{IC}. All these observations suggest the overall system dynamics being controlled by the breaking and making of ion cages, that is, the counterions leaving the ionic solvation sphere of the reference ion. Thus, the water−ion solvation structure, dynamics, and interplay among Li^+, NTf_2^-, and water molecules aid in the atomistic interpretation and help to strategize faster system dynamics by minimizing the ion-cage lifetimes that might also open up new research avenues in battery electrolytes.[124,125]

■ ASSOCIATED CONTENT

Supporting Information

The Supporting Information is available free of charge at https://pubs.acs.org/doi/10.1021/acs.jpcb.2c04391.

Non-bonded force field parameters for HOD, H_2O, Li^+, and NTf_2^- ions and density and box length of all systems based on the last 20 ns trajectory of the NPT run (PDF)

■ AUTHOR INFORMATION

Corresponding Author

Bhabani S. Mallik − *Department of Chemistry, Indian Institute of Technology Hyderabad, Sangareddy 502285 Telangana, India;* orcid.org/0000-0001-9657-1497; Phone: +914023016258; Email: bhabani@chy.iith.ac.in; Fax: +91 40 2301 6003

Author

Aritri Biswas − *Department of Chemistry, Indian Institute of Technology Hyderabad, Sangareddy 502285 Telangana, India;* orcid.org/0000-0003-1021-5550

Complete contact information is available at: https://pubs.acs.org/10.1021/acs.jpcb.2c04391

Notes

The authors declare no competing financial interest.

■ ACKNOWLEDGMENTS

A.B. would like to thank the Ministry of Education, India, for her Ph.D. fellowship.

■ REFERENCES

(1) Whittingham, M. S. Lithium Batteries and Cathode Materials. *Chem. Rev.* **2004**, *104*, 4271−4302.

(2) Armand, M.; Tarascon, J.-M. Building better batteries. *Nature* **2008**, *451*, 652−657.

(3) Ji, M.; Park, S.; Gaffney, K. J. Dynamics of Ion Assembly in Solution: 2DIR Spectroscopy Study of LiNCS in Benzonitrile. *J. Phys. Chem. Lett.* **2010**, *1*, 1771−1775.

(4) Manthiram, A. An Outlook on Lithium Ion Battery Technology. *ACS Cent. Sci.* **2017**, *3*, 1063−1069.

(5) Cheng, L.; Curtiss, L. A.; Zavadil, K. R.; Gewirth, A. A.; Shao, Y.; Gallagher, K. G. Sparingly Solvating Electrolytes for High Energy Density Lithium−Sulfur Batteries. *ACS Energy Lett.* **2016**, *1*, 503−509.

(6) Kartha, T. R.; Mallik, B. S. Ionic conductance and viscous drag in water-in-salt electrolytes for lithium and sodium ion batteries and supercapacitors. *Mater. Today Commun.* **2020**, *25*, 101588.

(7) Jiang, B.; Ponnuchamy, V.; Shen, Y.; Yang, X.; Yuan, K.; Vetere, V.; Mossa, S.; Skarmoutsos, I.; Zhang, Y.; Zheng, J. The Anion Effect on Li+ Ion Coordination Structure in Ethylene Carbonate Solutions. *J. Phys. Chem. Lett.* **2016**, *7*, 3554−3559.

(8) Armand, M.; Endres, F.; MacFarlane, D. R.; Ohno, H.; Scrosati, B. Ionic-liquid materials for the electrochemical challenges of the future. *Nat. Mater.* **2009**, *8*, 621−629.

(9) Yuan, K.; Bian, H.; Shen, Y.; Jiang, B.; Li, J.; Zhang, Y.; Chen, H.; Zheng, J. Coordination Number of Li+ in Nonaqueous Electrolyte Solutions Determined by Molecular Rotational Measurements. *J. Phys. Chem. B* **2014**, *118*, 3689−3695.

(10) Liu, X.; Yu, Z.; Sarnello, E.; Qian, K.; Seifert, S.; Winans, R. E.; Cheng, L.; Li, T. Microscopic Understanding of the Ionic Networks of "Water-in-Salt" Electrolytes with Synchrotron X-Ray Scattering. *Meet. Abstr.* **2021**, *MA2021-01*, 432.

(11) Dunn, B.; Kamath, H.; Tarascon, J.-M. Electrical Energy Storage for the Grid: A Battery of Choices. *Science* **2011**, *334*, 928−935.

(12) Wu, X.; Song, K.; Zhang, X.; Hu, N.; Li, L.; Li, W.; Zhang, L.; Zhang, H. Safety Issues in Lithium Ion Batteries: Materials and Cell Design. *Front. Energy Res.* **2019**, *7*, 65.

(13) Azeez, F.; Fedkiw, P. S. Conductivity of libob-based electrolyte for lithium-ion batteries. *J. Power Sources* **2010**, *195*, 7627−7633.

(14) Fulfer, K. D.; Kuroda, D. G. Solvation Structure and Dynamics of the Lithium Ion in Organic Carbonate-Based Electrolytes: A Time-Dependent Infrared Spectroscopy Study. *J. Phys. Chem. C* **2016**, *120*, 24011−24022.

(15) MacFarlane, D. R.; Forsyth, M.; Howlett, P. C.; Kar, M.; Passerini, S.; Pringle, J. M.; Ohno, H.; Watanabe, M.; Yan, F.; Zheng, W.; et al. Ionic liquids and their solid-state analogues as materials for energy generation and storage. *Nat. Rev. Mater.* **2016**, *1*, 15005.

(16) Serva, A.; Dubouis, N.; Grimaud, A.; Salanne, M. Confining Water in Ionic and Organic Solvents to Tune Its Adsorption and Reactivity at Electrified Interfaces. *Acc. Chem. Res.* **2021**, *54*, 1034−1042.

(17) Liang, T.; Hou, R.; Dou, Q.; Zhang, H.; Yan, X. The Applications of Water-in-Salt Electrolytes in Electrochemical Energy Storage Devices. *Adv. Funct. Mater.* **2021**, *31*, 2006749.

(18) Wang, Y.; Yi, J.; Xia, Y. Recent Progress in Aqueous Lithium-Ion Batteries. *Adv. Energy Mater.* **2012**, *2*, 830−840.

(19) Kim, H.; Hong, J.; Park, K.-Y.; Kim, H.; Kim, S.-W.; Kang, K. Aqueous Rechargeable Li and Na Ion Batteries. *Chem. Rev.* **2014**, *114*, 11788−11827.

(20) Suo, L.; Borodin, O.; Gao, T.; Olguin, M.; Ho, J.; Fan, X.; Luo, C.; Wang, C.; Xu, K. "Water-in-salt" electrolyte enables high-voltage aqueous lithium-ion chemistries. *Science* **2015**, *350*, 938−943.

(21) Wang, Y.; Meng, X.; Sun, J.; Liu, Y.; Hou, L. Recent Progress in "Water-in-Salt" Electrolytes Toward Non-lithium Based Rechargeable Batteries. *Front. Chem.* **2020**, *8*, 595.

(22) Yamada, Y.; Yaegashi, M.; Abe, T.; Yamada, A. A super-concentrated ether electrolyte for fast-charging Li-ion batteries. *Chem. Commun.* **2013**, *49*, 11194−11196.

(23) Yamada, Y.; Usui, K.; Sodeyama, K.; Ko, S.; Tateyama, Y.; Yamada, A. Hydrate-melt electrolytes for high-energy-density aqueous batteries. *Nat. Energy* **2016**, *1*, 16129.
(24) Franco, A. A. Multiscale modelling and numerical simulation of rechargeable lithium ion batteries: concepts, methods and challenges. *RSC Adv.* **2013**, *3*, 13027−13058.
(25) Shi, S.; Gao, J.; Liu, Y.; Zhao, Y.; Wu, Q.; Ju, W.; Ouyang, C.; Xiao, R. Multi-scale computation methods: Their applications in lithium-ion battery research and development. *Chin. Phys. B* **2016**, *25*, 018212.
(26) Li, Z.; Bouchal, R.; Mendez-Morales, T.; Rollet, A.-L.; Rizzi, C.; Le Vot, S.; Favier, F.; Rotenberg, B.; Borodin, O.; Fontaine, O.; et al. Transport Properties of Li-TFSI Water-in-Salt Electrolytes. *J. Phys. Chem. B* **2019**, *123*, 10514−10521.
(27) Borodin, O.; Suo, L.; Gobet, M.; Ren, X.; Wang, F.; Faraone, A.; Peng, J.; Olguin, M.; Schroeder, M.; Ding, M. S.; et al. Liquid Structure with Nano-Heterogeneity Promotes Cationic Transport in Concentrated Electrolytes. *ACS Nano* **2017**, *11*, 10462−10471.
(28) Lim, J.; Park, K.; Lee, H.; Kim, J.; Kwak, K.; Cho, M. Nanometric Water Channels in Water-in-Salt Lithium Ion Battery Electrolyte. *J. Am. Chem. Soc.* **2018**, *140*, 15661−15667.
(29) Han, S. Dynamic features of water molecules in super-concentrated aqueous electrolytes. *Sci. Rep.* **2018**, *8*, 9347.
(30) Kim, J.; Koo, B.; Lim, J.; Jeon, J.; Lim, C.; Lee, H.; Kwak, K.; Cho, M. Dynamic Water Promotes Lithium-Ion Transport in Superconcentrated and Eutectic Aqueous Electrolytes. *ACS Energy Lett.* **2021**, *7*, 189−196.
(31) Pauric, A. D.; Halalay, I. C.; Goward, G. R. Combined NMR and molecular dynamics modeling study of transport properties in sulfonamide based deep eutectic lithium electrolytes: LiTFSI based binary systems. *Phys. Chem. Chem. Phys.* **2016**, *18*, 6657−6667.
(32) Dou, Q.; Lei, S.; Wang, D.-W.; Zhang, Q.; Xiao, D.; Guo, H.; Wang, A.; Yang, H.; Li, Y.; Shi, S.; Yan, X. Safe and high-rate supercapacitors based on an "acetonitrile/water in salt" hybrid electrolyte. *Energy Environ. Sci.* **2018**, *11*, 3212−3219.
(33) Li, T.; Senesi, A. J.; Lee, B. Small Angle X-ray Scattering for Nanoparticle Research. *Chem. Rev.* **2016**, *116*, 11128−11180.
(34) Yu, Z.; Curtiss, L. A.; Winans, R. E.; Zhang, Y.; Li, T.; Cheng, L. Asymmetric Composition of Ionic Aggregates and the Origin of High Correlated Transference Number in Water-in-Salt Electrolytes. *J. Phys. Chem. Lett.* **2020**, *11*, 1276−1281.
(35) Zhang, Y.; Maginn, E. J. The effect of C2 substitution on melting point and liquid phase dynamics of imidazolium based-ionic liquids: insights from molecular dynamics simulations. *Phys. Chem. Chem. Phys.* **2012**, *14*, 12157−12164.
(36) Yu, G.; Zhao, D.; Wen, L.; Yang, S.; Chen, X. Viscosity of ionic liquids: Database, observation, and quantitative structure-property relationship analysis. *AIChE J.* **2012**, *58*, 2885−2899.
(37) Ren, Z.; Ivanova, A. S.; Couchot-Vore, D.; Garrett-Roe, S. Ultrafast Structure and Dynamics in Ionic Liquids: 2D-IR Spectroscopy Probes the Molecular Origin of Viscosity. *J. Phys. Chem. Lett.* **2014**, *5*, 1541−1546.
(38) Zhang, Y.; Maginn, E. J. Direct Correlation between Ionic Liquid Transport Properties and Ion Pair Lifetimes: A Molecular Dynamics Study. *J. Phys. Chem. Lett.* **2015**, *6*, 700−705.
(39) Kohagen, M.; Brehm, M.; Lingscheid, Y.; Giernoth, R.; Sangoro, J.; Kremer, F.; Naumov, S.; Iacob, C.; Kärger, J.; Valiullin, R.; et al. How Hydrogen Bonds Influence the Mobility of Imidazolium-Based Ionic Liquids. A Combined Theoretical and Experimental Study of 1-n-Butyl-3-methylimidazolium Bromide. *J. Phys. Chem. B* **2011**, *115*, 15280−15288.
(40) Kohagen, M.; Brehm, M.; Thar, J.; Zhao, W.; Müller-Plathe, F.; Kirchner, B. Performance of Quantum Chemically Derived Charges and Persistence of Ion Cages in Ionic Liquids. A Molecular Dynamics Simulations Study of 1-n-Butyl-3-methylimidazolium Bromide. *J. Phys. Chem. B* **2011**, *115*, 693−702.
(41) Lee, S. H.; Rasaiah, J. C. Molecular Dynamics Simulation of Ion Mobility. 2. Alkali Metal and Halide Ions Using the SPC/E Model for Water at 25 °C. *J. Phys. Chem.* **1996**, *100*, 1420−1425.
(42) Canongia Lopes, J. N.; Pádua, A. A. H. Molecular Force Field for Ionic Liquids Composed of Triflate or Bistriflylimide Anions. *J. Phys. Chem. B* **2004**, *108*, 16893−16898.
(43) Wu, Y.; Tepper, H. L.; Voth, G. A. Flexible simple point-charge water model with improved liquid-state properties. *J. Chem. Phys.* **2006**, *124*, 024503.
(44) Paesani, F.; Zhang, W.; Case, D. A.; Cheatham, T. E.; Voth, G. A. An accurate and simple quantum model for liquid water. *J. Chem. Phys.* **2006**, *125*, 184507.
(45) Frisch, M. J.; Trucks, G. W.; Schlegel, H. B.; Scuseria, G. E.; Robb, M. A.; Cheeseman, J. R.; Scalmani, G.; Barone, V.; Mennucci, B.; Petersson, G. A.; et al.*Gaussian 09*; Revision D.01.
(46) Martínez, L.; Andrade, R.; Birgin, E. G.; Martínez, J. M. PACKMOL: a package for building initial configurations for molecular dynamics simulations. *J. Comput. Chem.* **2009**, *30*, 2157−2164.
(47) Payne, M. C.; Teter, M. P.; Allan, D. C.; Arias, T. A.; Joannopoulos, J. D. Iterative minimization techniques for ab initio total-energy calculations: molecular dynamics and conjugate gradients. *Rev. Mod. Phys.* **1992**, *64*, 1045−1097.
(48) Essmann, U.; Perera, L.; Berkowitz, M. L.; Darden, T.; Lee, H.; Pedersen, L. G. A smooth particle mesh Ewald method. *J. Chem. Phys.* **1995**, *103*, 8577−8593.
(49) Darden, T.; York, D.; Pedersen, L. Particle mesh Ewald: An N·log(N) method for Ewald sums in large systems. *J. Chem. Phys.* **1993**, *98*, 10089−10092.
(50) York, D. M.; Darden, T. A.; Pedersen, L. G. The effect of long-range electrostatic interactions in simulations of macromolecular crystals: A comparison of the Ewald and truncated list methods. *J. Chem. Phys.* **1993**, *99*, 8345−8348.
(51) Verlet, L. Computer "Experiments" on Classical Fluids. I. Thermodynamical Properties of Lennard-Jones Molecules. *Phys. Rev.* **1967**, *159*, 98−103.
(52) Bussi, G.; Donadio, D.; Parrinello, M. Canonical sampling through velocity rescaling. *J. Chem. Phys.* **2007**, *126*, 014101.
(53) Parrinello, M.; Rahman, A. Polymorphic transitions in single crystals: A new molecular dynamics method. *J. Appl. Phys.* **1981**, *52*, 7182−7190.
(54) Hess, B.; Bekker, H.; Berendsen, H. J. C.; Fraaije, J. G. E. M. LINCS: A linear constraint solver for molecular simulations. *J. Comput. Chem.* **1997**, *18*, 1463−1472.
(55) Daubechies, I. The wavelet transform, time-frequency localization and signal analysis. *IEEE Trans. Inf. Theor.* **1990**, *36*, 961−1005.
(56) Vela-arevalo, L. V.; Wiggins, S. Time-frequency analysis of classical trajectories of polyatomic molecules. *Int. J. Bifurcation Chaos Appl. Sci. Eng.* **2001**, *11*, 1359−1380.
(57) Berendsen, H. J. C.; van der Spoel, D.; van Drunen, R. GROMACS: A message-passing parallel molecular dynamics implementation. *Comput. Phys. Commun.* **1995**, *91*, 43−56.
(58) Van Der Spoel, D.; Lindahl, E.; Hess, B.; Groenhof, G.; Mark, A. E.; Berendsen, H. J. C. GROMACS: fast, flexible, and free. *J. Comput. Chem.* **2005**, *26*, 1701−1718.
(59) Abraham, M. J.; Murtola, T.; Schulz, R.; Páll, S.; Smith, J. C.; Hess, B.; Lindahl, E. GROMACS: High performance molecular simulations through multi-level parallelism from laptops to supercomputers. *SoftwareX* **2015**, *1−2*, 19−25.
(60) Laskar, J.; Froeschlé, C.; Celletti, A. The measure of chaos by the numerical analysis of the fundamental frequencies. Application to the standard mapping. *Phys. D* **1992**, *56*, 253−269.
(61) Laskar, J. Frequency analysis for multi-dimensional systems. Global dynamics and diffusion. *Phys. D* **1993**, *67*, 257−281.
(62) Mallik, B. S.; Semparithi, A.; Chandra, A. Vibrational Spectral Diffusion and Hydrogen Bond Dynamics in Heavy Water from First Principles. *J. Phys. Chem. A* **2008**, *112*, 5104−5112.
(63) Biswas, A.; Priyadarsini, A.; Mallik, B. S. Dynamics and Spectral Response of Water Molecules around Tetramethylammonium Cation. *J. Phys. Chem. B* **2019**, *123*, 8753−8766.

https://doi.org/10.1021/acs.jpcb.2c04391
J. Phys. Chem. B 2023, 127, 236−248

(64) Mallik, B. S.; Semparithi, A.; Chandra, A. A first principles theoretical study of vibrational spectral diffusion and hydrogen bond dynamics in aqueous ionic solutions: D2O in hydration shells of Cl− ions. *J. Chem. Phys.* **2008**, *129*, 194512.
(65) Biswas, S.; Mallik, B. S. Ultrafast Vibrational Spectroscopy of Aqueous Solution of Methylamine from First Principles MD Simulations. *ChemistrySelect* **2017**, *2*, 74−83.
(66) Biswas, S.; Mallik, B. S. Time-dependent vibrational spectral analysis of first principles trajectory of methylamine with wavelet transform. *Phys. Chem. Chem. Phys.* **2017**, *19*, 9912−9922.
(67) Biswas, A.; Mallik, B. S. Ultrafast Aqueous Dynamics in Concentrated Electrolytic Solutions of Lithium Salt and Ionic Liquid. *J. Phys. Chem. B* **2020**, *124*, 9898−9912.
(68) Shatkay, H.*The Fourier Transform—A Primer*; Brown University: Providence, RI, USA, 1995.
(69) Carmona, R.; Hwang, W.-L.; Torresani, B.*Practical Time-Frequency Analysis: Gabor and Wavelet Transforms, with an Implementation in S*; Academic Press, 1998.
(70) Bankura, A.; Karmakar, A.; Carnevale, V.; Chandra, A.; Klein, M. L. Structure, Dynamics, and Spectral Diffusion of Water from First-Principles Molecular Dynamics. *J. Phys. Chem. C* **2014**, *118*, 29401−29411.
(71) Choudhuri, J. R.; Yadav, V. K.; Karmakar, A.; Mallik, B. S.; Chandra, A. A first-principles theoretical study of hydrogen-bond dynamics and vibrational spectral diffusion in aqueous ionic solution: Water in the hydration shell of a fluoride ion. *Pure Appl. Chem.* **2012**, *85*, 27−40.
(72) Biswas, S.; Mallik, B. S. Aqueous solvation of an amide molecule from first principles molecular simulations: Structure, hydrogen bond dynamics and spectral signature. *J. Mol. Liq.* **2015**, *212*, 941−946.
(73) Biswas, A.; Mallik, B. S. Ionic Dynamics and Vibrational Spectral Diffusion of a Protic Alkylammonium Ionic Salt through Intrinsic Cationic N−H Vibrational Probe from FPMD Simulations. *J. Phys. Chem. A* **2022**, *126*, 5134−5147.
(74) Biswas, A.; Mallik, B. S. Revisiting OD-stretching dynamics of methanol-d4, ethanol-d6 and dilute HOD/H2O mixture with predefined potentials and wavelet transform spectra. *Chem. Phys.* **2022**, *553*, 111385.
(75) Biswas, A.; Mallik, B. S. Vibrational spectral dynamics and ion-probe interactions of the hydrogen-bonded liquids in 1-ethyl-3-methylimidazolium bis(trifluoromethylsulfonyl)imide. *Chem. Phys.* **2022**, *559*, 111519.
(76) Biswas, A.; Mallik, B. S. Microheterogeneity-Induced Vibrational Spectral Dynamics of Aqueous 1-Alkyl-3-methylimidazolium Tetrafluoroborate Ionic Liquids of Different Cationic Chain Lengths. *J. Phys. Chem. B* **2022**, *126*, 5523−5533.
(77) Brehm, M.; Kirchner, B. TRAVIS - A Free Analyzer and Visualizer for Monte Carlo and Molecular Dynamics Trajectories. *J. Chem. Inf. Model.* **2011**, *51*, 2007−2023.
(78) Ueno, K.; Yoshida, K.; Tsuchiya, M.; Tachikawa, N.; Dokko, K.; Watanabe, M. Glyme−Lithium Salt Equimolar Molten Mixtures: Concentrated Solutions or Solvate Ionic Liquids? *J. Phys. Chem. B* **2012**, *116*, 11323−11331.
(79) Park, J.-W.; Yamauchi, K.; Takashima, E.; Tachikawa, N.; Ueno, K.; Dokko, K.; Watanabe, M. Solvent Effect of Room Temperature Ionic Liquids on Electrochemical Reactions in Lithium−Sulfur Batteries. *J. Phys. Chem. C* **2013**, *117*, 4431−4440.
(80) Suo, L.; Hu, Y.-S.; Li, H.; Armand, M.; Chen, L. A new class of Solvent-in-Salt electrolyte for high-energy rechargeable metallic lithium batteries. *Nat. Commun.* **2013**, *4*, 1481.
(81) Chandrasekhar, J.; Spellmeyer, D. C.; Jorgensen, W. L. Energy component analysis for dilute aqueous solutions of lithium(1+), sodium(1+), fluoride(1-), and chloride(1-) ions. *J. Am. Chem. Soc.* **1984**, *106*, 903−910.
(82) Dubouis, N.; Lemaire, P.; Mirvaux, B.; Salager, E.; Deschamps, M.; Grimaud, A. The role of the hydrogen evolution reaction in the solid−electrolyte interphase formation mechanism for "Water-in-Salt" electrolytes. *Energy Environ. Sci.* **2018**, *11*, 3491−3499.
(83) Zheng, J.; Tan, G.; Shan, P.; Liu, T.; Hu, J.; Feng, Y.; Yang, L.; Zhang, M.; Chen, Z.; Lin, Y.; et al. Understanding Thermodynamic and Kinetic Contributions in Expanding the Stability Window of Aqueous Electrolytes. *Chem* **2018**, *4*, 2872−2882.
(84) Zhang, M.; Hao, H.; Zhou, D.; Duan, Y.; Wang, Y.; Bian, H. Understanding the Microscopic Structure of a "Water-in-Salt" Lithium Ion Battery Electrolyte Probed with Ultrafast IR Spectroscopy. *J. Phys. Chem. C* **2020**, *124*, 8594−8604.
(85) Omta, A. W.; Kropman, M. F.; Woutersen, S.; Bakker, H. J. Negligible effect of ions on the hydrogen-bond structure in liquid water. *Science* **2003**, *301*, 347−349.
(86) Moilanen, D. E.; Wong, D.; Rosenfeld, D. E.; Fenn, E. E.; Fayer, M. D. Ion−water hydrogen-bond switching observed with 2D IR vibrational echo chemical exchange spectroscopy. *Proc. Natl. Acad. Sci. U.S.A.* **2009**, *106*, 375−380.
(87) Deàk, J. C.; Rhea, S. T.; Iwaki, L.; Dlott, D. D. Vibrational Energy Relaxation and Spectral Diffusion in Water and Deuterated Water. *J. Phys. Chem. A* **2000**, *104*, 4866−4875.
(88) Corcelli, S. A.; Lawrence, C. P.; Asbury, J. B.; Steinel, T.; Fayer, M. D.; Skinner, J. L. Spectral diffusion in a fluctuating charge model of water. *J. Chem. Phys.* **2004**, *121*, 8897−8900.
(89) Asbury, J. B.; Steinel, T.; Stromberg, C.; Corcelli, S. A.; Lawrence, C. P.; Skinner, J. L.; Fayer, M. D. Water Dynamics: Vibrational Echo Correlation Spectroscopy and Comparison to Molecular Dynamics Simulations. *J. Phys. Chem. A* **2004**, *108*, 1107−1119.
(90) Biswas, A.; Mallik, B. S. Conformation-induced vibrational spectral dynamics of hydrogen peroxide and vicinal water molecules. *Phys. Chem. Chem. Phys.* **2021**, *23*, 6665−6676.
(91) Biswas, A.; Mallik, B. S. 2D IR spectra of the intrinsic vibrational probes of ionic liquid from dispersion corrected DFT-MD simulations. *J. Mol. Liq.* **2022**, *348*, 118390.
(92) Ren, Z.; Brinzer, T.; Dutta, S.; Garrett-Roe, S. Thiocyanate as a Local Probe of Ultrafast Structure and Dynamics in Imidazolium-Based Ionic Liquids: Water-Induced Heterogeneity and Cation-Induced Ion Pairing. *J. Phys. Chem. B* **2015**, *119*, 4699−4712.
(93) Tamimi, A.; Bailey, H. E.; Fayer, M. D. Alkyl Chain Length Dependence of the Dynamics and Structure in the Ionic Regions of Room-Temperature Ionic Liquids. *J. Phys. Chem. B* **2016**, *120*, 7488−7501.
(94) Yamada, S. A.; Bailey, H. E.; Tamimi, A.; Li, C.; Fayer, M. D. Dynamics in a Room-Temperature Ionic Liquid from the Cation Perspective: 2D IR Vibrational Echo Spectroscopy. *J. Am. Chem. Soc.* **2017**, *139*, 2408−2420.
(95) Giammanco, C. H.; Kramer, P. L.; Yamada, S. A.; Nishida, J.; Tamimi, A.; Fayer, M. D. Carbon dioxide in an ionic liquid: Structural and rotational dynamics. *J. Chem. Phys.* **2016**, *144*, 104506.
(96) Giammanco, C. H.; Yamada, S. A.; Kramer, P. L.; Tamimi, A.; Fayer, M. D. Structural and Rotational Dynamics of Carbon Dioxide in 1-Alkyl-3-methylimidazolium Bis(trifluoromethylsulfonyl)imide Ionic Liquids: The Effect of Chain Length. *J. Phys. Chem. B* **2016**, *120*, 6698−6711.
(97) Williams, I. M.; Qasim, L. N.; Tran, L.; Scott, A.; Riley, K.; Dutta, S. C-D Vibration at C2 Position of Imidazolium Cation as a Probe of the Ionic Liquid Microenvironment. *J. Phys. Chem. A* **2019**, *123*, 6342−6349.
(98) Biswas, A.; Mallik, B. S. Dynamics of Ionic Liquid through Intrinsic Vibrational Probes Using the Dispersion-Corrected DFT Functionals. *J. Phys. Chem. B* **2021**, *125*, 6994−7008.
(99) Biswas, A.; Mallik, B. S. Structure and stretching dynamics of water molecules around an amphiphilic amide from FPMD simulations: A case study of N,N-dimethylformamide. *J. Mol. Liq.* **2020**, *302*, 112524.
(100) Biswas, A.; Mallik, B. S. Conformational dynamics of aqueous hydrogen peroxide from first principles molecular dynamics simulations. *Phys. Chem. Chem. Phys.* **2020**, *22*, 28286−28296.
(101) Biswas, A.; Mallik, B. S. Distinctive behavior and two-dimensional vibrational dynamics of water molecules inside glycine solvation shell. *RSC Adv.* **2020**, *10*, 6658−6670.

https://doi.org/10.1021/acs.jpcb.2c04391
J. Phys. Chem. B 2023, 127, 236−248

(102) Biswas, A.; Mallik, B. S. Conformation-induced vibrational spectral dynamics of hydrogen peroxide and vicinal water molecules. *Phys. Chem. Chem. Phys.* **2021**, *23*, 6665−6676.
(103) Biswas, A.; Dasari, S.; Mallik, B. S. Cohesiveness and Nondiffusive Rotational Jump Dynamics of Protic Ionic Liquid from Dispersion-Corrected FPMD Simulations. *J. Phys. Chem. B* **2020**, *124*, 10752−10765.
(104) Priyadarshini, A.; Biswas, A.; Chakraborty, D.; Mallik, B. S. Structural and Thermophysical Anomalies of Liquid Water: A Tale of Molecules in the Instantaneous Low- and High-Density Regions. *J. Phys. Chem. B* **2020**, *124*, 1071−1081.
(105) Dorbritz, S.; Ruth, W.; Kragl, U. Investigation on Aggregate Formation of Ionic Liquids. *Adv. Synth. Catal.* **2005**, *347*, 1273−1279.
(106) Köddermann, T.; Klembt, S.; Klasen, D.; Paschek, D.; Kragl, U.; Ludwig, R. The effect of neutral ion aggregate formation on the electrical conductivity of an ionic liquid and its mixtures with chloroform. *Chemphyschem* **2012**, *13*, 1748−1752.
(107) Chowdhuri, S.; Chandra, A. Molecular dynamics simulations of aqueous NaCl and KCl solutions: Effects of ion concentration on the single-particle, pair, and collective dynamical properties of ions and water molecules. *J. Chem. Phys.* **2001**, *115*, 3732−3741.
(108) Balasubramanian, S.; Pal, S.; Bagchi, B. Hydrogen-Bond Dynamics near a Micellar Surface: Origin of the Universal Slow Relaxation at Complex Aqueous Interfaces. *Phys. Rev. Lett.* **2002**, *89*, 115505.
(109) Zhao, W.; Leroy, F.; Heggen, B.; Zahn, S.; Kirchner, B.; Balasubramanian, S.; Müller-Plathe, F. Are There Stable Ion-Pairs in Room-Temperature Ionic Liquids? Molecular Dynamics Simulations of 1-n-Butyl-3-methylimidazolium Hexafluorophosphate. *J. Am. Chem. Soc.* **2009**, *131*, 15825−15833.
(110) Kirchner, B.; Malberg, F.; Firaha, D. S.; Hollóczki, O. Ion pairing in ionic liquids. *J. Phys. Condens. Matter* **2015**, *27*, 463002.
(111) Kartha, T. R.; Reddy, D. N.; Mallik, B. S. Insights into the structure and ionic transport in "water-in-bisalt" electrolytes for lithium-ion batteries. *Mater. Adv.* **2021**, *2*, 7691−7700.
(112) Luzar, A.; Chandler, D. Hydrogen-bond kinetics in liquid water. *Nature* **1996**, *379*, 55−57.
(113) Luzar, A.; Chandler, D. Effect of Environment on Hydrogen Bond Dynamics in Liquid Water. *Phys. Rev. Lett.* **1996**, *76*, 928−931.
(114) Luzar, A. Resolving the hydrogen bond dynamics conundrum. *J. Chem. Phys.* **2000**, *113*, 10663−10675.
(115) Wong, D. B.; Giammanco, C. H.; Fenn, E. E.; Fayer, M. D. Dynamics of Isolated Water Molecules in a Sea of Ions in a Room Temperature Ionic Liquid. *J. Phys. Chem. B* **2013**, *117*, 623−635.
(116) Terranova, Z. L.; Corcelli, S. A. Molecular Dynamics Investigation of the Vibrational Spectroscopy of Isolated Water in an Ionic Liquid. *J. Phys. Chem. B* **2014**, *118*, 8264−8272.
(117) Ji, M.; Odelius, M.; Gaffney, K. J. Large Angular Jump Mechanism Observed for Hydrogen Bond Exchange in Aqueous Perchlorate Solution. *Science* **2010**, *328*, 1003−1005.
(118) Reddy, Th. D. N.; Mallik, B. S. Connecting Correlated and Uncorrelated Transport to Dynamics of Ionic Interactions in Cyclic Ammonium-Based Ionic Liquids. *J. Phys. Chem. B* **2020**, *124*, 6813−6824.
(119) Gehrke, S.; von Domaros, M.; Clark, R.; Hollóczki, O.; Brehm, M.; Welton, T.; Luzar, A.; Kirchner, B. Structure and lifetimes in ionic liquids and their mixtures. *Faraday Discuss.* **2018**, *206*, 219−245.
(120) Cammarata, L.; Kazarian, S. G.; Salter, P. A.; Welton, T. Molecular states of water in room temperature ionic liquids. *Phys. Chem. Chem. Phys.* **2001**, *3*, 5192−5200.
(121) Giammanco, C. H.; Kramer, P. L.; Fayer, M. D. Ionic Liquid versus Li+ Aqueous Solutions: Water Dynamics near Bistriflimide Anions. *J. Phys. Chem. B* **2016**, *120*, 9997−10009.
(122) Shi, R.; Wang, Y. Ion-Cage Interpretation for the Structural and Dynamic Changes of Ionic Liquids under an External Electric Field. *J. Phys. Chem. B* **2013**, *117*, 5102−5112.
(123) Jeon, J.; Cho, M. Ion Transport in Super-Concentrated Aqueous Electrolytes for Lithium-Ion Batteries. *J. Phys. Chem. C* **2021**, *125*, 23622−23633.
(124) Lin, C.-H.; Sun, K.; Ge, M.; Housel, L. M.; McCarthy, A. H.; Vila, M. N.; Zhao, C.; Xiao, X.; Lee, W.-K.; Takeuchi, K. J.; et al. Systems-level investigation of aqueous batteries for understanding the benefit of water-in-salt electrolyte by synchrotron nanoimaging. *Sci. Adv.* **2020**, *6*, No. eaay7129.
(125) Shen, Y.; Liu, B.; Liu, X.; Liu, J. J.; Ding, C.; Zhong, W.; Hu, W. Water-in-salt electrolyte for safe and high-energy aqueous battery. *Energy Storage Mater.* **2021**, *34*, 461−474.

https://doi.org/10.1021/acs.jpcb.2c04391
J. Phys. Chem. B 2023, 127, 236−248